



LAWRENCE
LIVERMORE
NATIONAL
LABORATORY

Contrast analysis and stability on the ExAO testbed

Julia Evans, Sandrine Thomas, Donald Gavel,
Daren Dillon, Bruce Macintosh

June 12, 2008

SPIE Astronomical Telescopes and Instrumentation 2008
Marseille, France
June 23, 2008 through June 28, 2008

Disclaimer

This document was prepared as an account of work sponsored by an agency of the United States government. Neither the United States government nor Lawrence Livermore National Security, LLC, nor any of their employees makes any warranty, expressed or implied, or assumes any legal liability or responsibility for the accuracy, completeness, or usefulness of any information, apparatus, product, or process disclosed, or represents that its use would not infringe privately owned rights. Reference herein to any specific commercial product, process, or service by trade name, trademark, manufacturer, or otherwise does not necessarily constitute or imply its endorsement, recommendation, or favoring by the United States government or Lawrence Livermore National Security, LLC. The views and opinions of authors expressed herein do not necessarily state or reflect those of the United States government or Lawrence Livermore National Security, LLC, and shall not be used for advertising or product endorsement purposes.

Contrast analysis and stability on the ExAO testbed

Julia W. Evans^a, Sandrine Thomas^b, Donald Gavel^b, Daren Dillon^b, Bruce Macintosh^{a,b}

^aLawrence Livermore National Laboratory, 7000 East Avenue, Livermore, USA

^bUCO Lick Observatory, Laboratory for Adaptive Optics, University of California at Santa Cruz, 1156 High St., Santa Cruz, CA, 95064

ABSTRACT

High-contrast adaptive optics systems, such as those needed to image extrasolar planets, are known to require excellent wavefront control and diffraction suppression. The Laboratory for Adaptive Optics at UC Santa Cruz is investigating limits to high-contrast imaging in support of the Gemini Planet Imager. Previous contrast measurements were made with a simple single-opening prolate spheroid shaped pupil that produced a limited region of high-contrast, particularly when wavefront errors were corrected with the 1024-actuator Boston Micromachines MEMS deformable mirror currently in use on the testbed. A more sophisticated shaped pupil is now being used that has a much larger region of interest facilitating a better understanding of high-contrast measurements. In particular we examine the effect of heat sources in the testbed on PSF stability. We find that rms image motion scales as $0.02 \lambda/D$ per watt when the heat source is near the pupil plane. As a result heat sources of greater than 5 watts should be avoided near pupil planes for GPI. The safest place to introduce heat is near a focal plane. Heat also can effect the standard deviation of the high-contrast region but in the final instrument other sources of error should be more significant.

Keywords: Adaptive Optics, MEMS, Extreme Adaptive Optics, High-contrast imaging, Coronagraphy

1. INTRODUCTION

Imaging extrasolar planets is a technically challenging but crucial step in the study of planet formation and planetary science. Imaging young Jupiter-like planets still glowing with the heat of formation will require contrasts of between 10^{-6} and 10^{-7} . High-contrast imaging requires suppressing diffraction and controlling wavefront errors. Laboratory tests investigating the experimental limits to contrast are ongoing at several institutions including the Extreme Adaptive Optics (ExAO) Testbed at the Laboratory for Adaptive Optics (LAO) located at the University of California, Santa Cruz, which supports the Gemini Planet Imager (GPI).¹ This instrument, which has expected first light in 2010, will be deployed at Gemini Observatory to conduct a survey of giant planets. The SPHERE project also has a ground-based imager under development planned for first light in the same year² for the European Southern Observatory (ESO) Very Large Telescope (VLT). There is also interest in imaging planets from space. The Terrestrial Planet Finder (TPF) is a space-based instrument with more stringent contrast requirements for imaging earth-like planets. Testbed experiments in support of TPF are on-going on the High Contrast Imaging Testbed (HCIT)³ at the Jet Propulsion Laboratory (JPL).

Most experiments in high-contrast imaging have focused on suppressing diffraction and wavefront control. It is becoming clear that amplitude errors must also be considered, either in design choices or with active control.^{3,4} In the design of a planet imager there are other more practical concerns that can also be investigated using a high-contrast testbed. On the ExAO testbed we continue to investigate diffraction suppression and wavefront control, but this proceeding focuses on PSF stability, particularly the effect of small heat sources on that stability.

Most optical systems have heat sources, but in a testbed environment the system is usually spread out enough to avoid having heat sources directly under the beam. In an instrument design, particularly for a telescope with a cassegrain focus it is nearly unavoidable. Heat sources could effect PSF stability and ultimately limit contrast either by directly reducing image quality or by reducing the efficiency of post-processing techniques.

2. EXPERIMENTAL METHOD

The ExAO testbed is well suited to high-contrast experiments. High-contrast measurements have been recorded with a flat mirror and a MEMS mirror.^{5,6} The testbed can also operate in interferometry, or phase shifting diffraction interferometer (PSDI), mode. A 1024 MEMS DM⁷ was installed and closed loop performance was characterized with the PSDI as the wavefront sensor (WFS).⁸ The precision wavefront correction of < 1 nm over controllable spatial frequencies has yielded contrast of $\sim 10^{-6}$,⁶ while contrast with the flat is $\sim 10^{-7}$.⁵ Contrast on the testbed is generally limited by a combination of phase and amplitude. The original layout for the ExAO

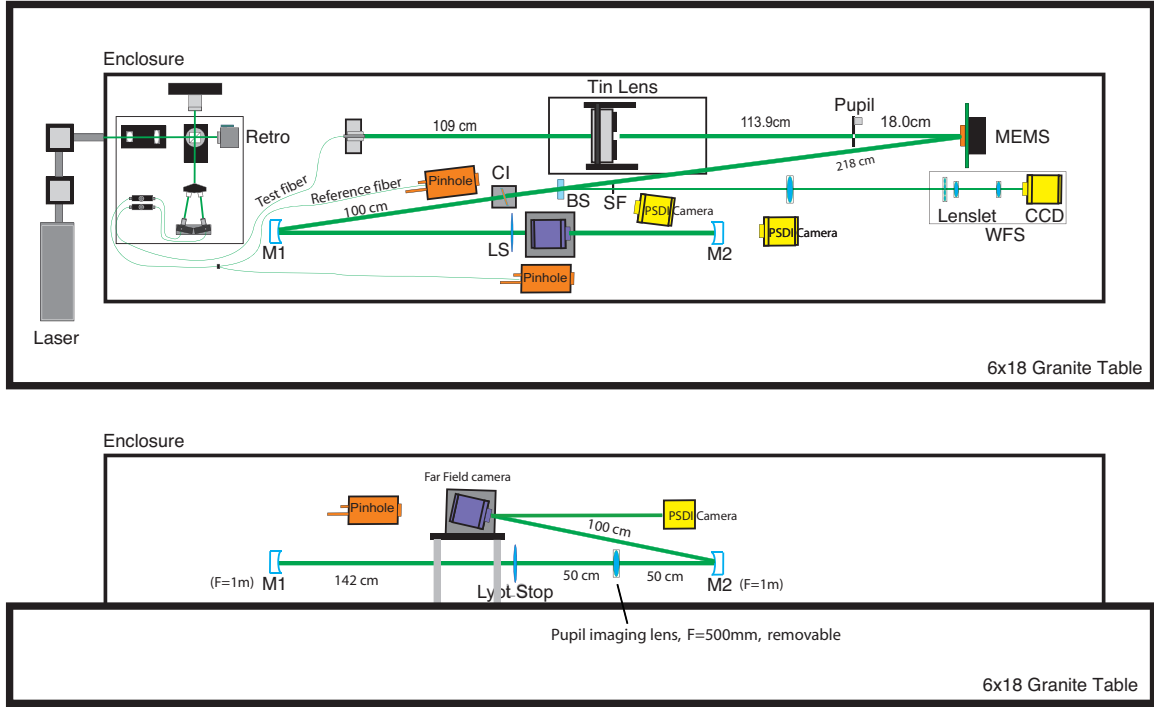


Figure 1. Schematic of the Phase II ExAO testbed. The PSDI front end located at the top left feeds the test (measurement) and reference fibers for the system. The far-field camera is out-of-plane to reduce astigmatism introduced by the spherical mirrors (M1 and M2). CI is the coronagraph input, or the first focal plane of the system and LS is the re-images pupil or the location of the Lyot stop for a Lyot-style coronagraph.

testbed is described in several publications.^{5,8} The system was later upgraded to include a spatially filtered wavefront sensor.⁹ In 2006 Phase II of the testbed was completed. In brief, the Phase I system was extended with two spherical mirrors to add an additional pupil and focal plane, allowing a more sophisticated lyot-style coronagraph for diffraction suppression. The second focal plane also makes far-field imaging with shaped pupils easier as the core of the PSF still needs to be blocked to increase dynamic range. Figure 1 is a schematic of the Phase II testbed. In the top left corner is the PSDI front end which feeds both the reference and the measurement (or test) beams. The two spherical mirrors used to re-image the pupil introduce astigmatism, and the far-field camera is placed out-of-plane to correct that error. The beam splitter (BS) before the first focus feeds the spatial filtered (SF) Shack-Hartman wavefront sensor (WFS), which was not used for the results presented here. The BS is frequently removed during far-field imaging to avoid ghost reflections that reduce contrast. While the results

presented here used a flat mirror, the system generally uses 1024 - actuator MEMS deformable mirror (DM), produced by Boston Micromachines. The first engineering grade 4096-actuator MEMS has been delivered and will eventually replace the 1024-actuator device in the system.

In imaging mode, the testbed consists of a laser source (532 nm) passed through an optical fiber and a high-quality lens (< 1 nm rms over a 50-mm beam size). The beam passes through a pupil stop, reflects off the DM (or a flat mirror), is brought to focus where the focal plane mask for the shaped pupil (or an occulter for a Lyot-style coronagraph) blocks the PSF core and then is re-imaged onto the CCD. The CCD is sampled at ~ 5 times the Nyquist limit. Diffraction is suppressed with a shaped pupil coronagraph.¹⁰ Previous high-contrast measurements were taken with simple single-opening prolate shaped pupil,⁵ but the multi-opening mask used here produces a much larger region of interest (ROI) (See Fig. 2). This larger ROI is particularly helpful for

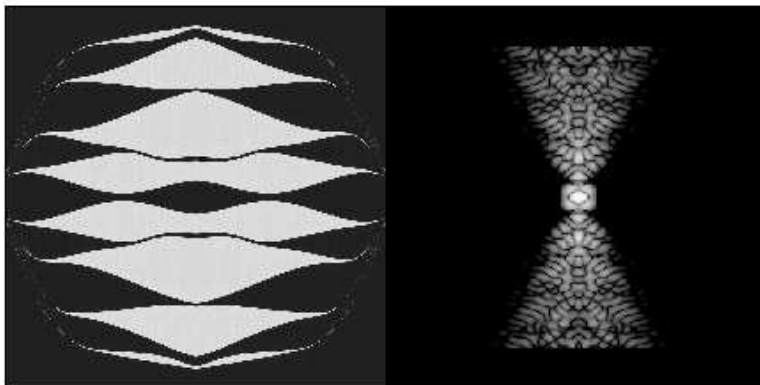


Figure 2. The shaped pupil coronagraph made by Princeton University^{11,12} is shown on the left with the corresponding high-contrast PSF on the right.

stability measurements as more of the speckle pattern is visible in each image. It should be noted that this more sophisticated design does not improve contrast, as contrast in our system is limited by a combination of phase and amplitude errors. Experiments are also underway with the apodized pupil lyot coronagraph^{13,14} that will be used for GPI and are presented in another paper in this volume.¹⁵ Preliminary contrast measurements with the APLC are quite promising and the APLC will likely replace shaped pupils for most new measurements.

Imaging mode is used to directly measure contrast, defined as the ratio of the intensity in the ROI (ROI) to the core intensity. High-contrast imaging on the ExAO testbed is typically done with two images, an unsaturated image of the core of the PSF and a saturated image with the core blocked by a focal plane mask to avoid saturating the CCD. The saturated image is normalized by the unsaturated peak value and the known scale factor produced by ND filters or integration time between the two images.

PSF stability on the ExAO testbed was assessed using a series of measurements over time of both unsaturated (un-occulted) far-field images and saturated images with a focal plane mask (to avoid CCD saturation). Neutral density filters were used to increase power by 5 orders of magnitude between un-occulted and occulted images. For each measurement 25 frames of 0.01s integration time were taken (about a second between each). This is the shortest shutter time of the far-field CCD. After systematic stability was measured (and improved) an additional variable heat source was introduced to the system. The heat source is a 25 watt resistor powered by a variable voltage supply. The resistor is mounted four inches below the beamline of the testbed (See Fig. 3). The source was placed 10 cm in front of the first pupil plane, directly in front of the MEMS DM plane (flat mirror in this case), near focus position 1, near the second pupil (Lyot) plane and between the input and output beams onto the MEMS 45 cm in front of the pupil plane. The voltage was varied to introduce between 0 and 15 watts of energy, which corresponds to a temperature change (of the resistor not the surrounding air) of 75° F to 313° F. The system was given 20 minutes to stabilize with each new heat setting. While systematic PSF stability was assessed without an additional heat source, the same time scales were used. In addition systematic stability

was measured over longer time scales. Measurements were taken over several hours and over night. Longer measurements of 100 frames were also used to look at more mid-term trends in image motion.

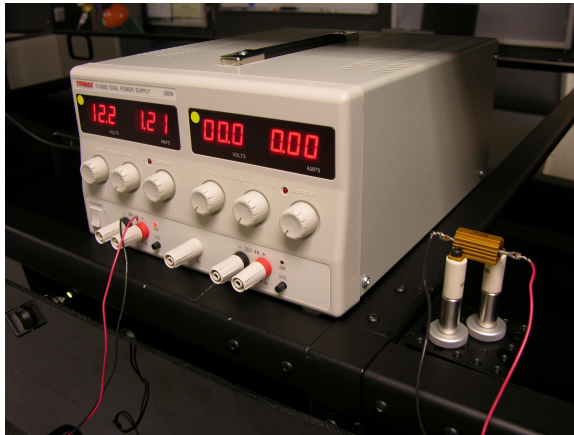


Figure 3. Picture of resistor and variable voltage supply used to introduce heat at various locations on the testbed.

3. RESULTS AND DISCUSSION

We are interested in PSF stability in the high-contrast regime. Figures 4 and 5 are typical of high-contrast measurements on the ExAO testbed. These measurements were made with the new more sophisticated shaped pupil. Figure 4 contains a high-contrast images measured with the new shaped pupil coronagraph on the ExAO testbed with a MEMS mirror (top) and the flat mirror (bottom). The radial average over 60 degrees of these images is shown in Fig. 5. Contrast with the flat mirror is better primarily because of amplitude errors introduced by the MEMS mirror. Also, the MEMS contrast measurements are slightly worse than previous measurements and the predicted contrast from the PSDI measured phase and amplitude. This could be caused by scattered light off of the pupil itself.

3.1 Stability of PSF core

In initial measurements systematic image motion was quite high, 0.5 pixels rms ($0.05 \lambda/D$). Comparison to older far-field measurements of 10 frames that are typically averaged indicated the system was more stable previously (0.1 pixels ($0.01 \lambda/D$) rms centroid motion). Vibration issues on the table were addressed and stability was returned to slightly better than the previous level. In the 100 frame measurements there appears to be a somewhat sinusoidal cycle in image motion leading to a variation in the rms of the 25 frame measurements. Typically the standard deviation is 0.1, but can go as low as 0.06 pixels rms (0.01 and $0.006 \lambda/D$ respectively). We think this variation is due to the overall sinusoidal trend. There are some differences between horizontal and vertical image motion. In general horizontal image motion is worse and for this analysis we focus on the horizontal direction as the worse case scenario.

The heat source discussed in Section 2 was introduced at multiple positions on the table and produced between 0 and 15 watts of heat. Both position and power matter when determining the effect on image motion. Placing the source in front of the pupil plane or the lyot-plane (a re-imaged smaller pupil) introduces the most image motion. The effect is surprisingly linear in the horizontal centroids (See Fig. 7). For a heat source near the pupil plane the standard deviation of image motion increases by about $0.02 \lambda/D$ per watt. Image motion less than $0.1 \lambda/D$ is probably insignificant, so levels of greater than 5 watts should be avoided in close proximity to the pupil plane. There is also an effect when heat is introduced in the front of the MEMS plane (about 18 cm behind the pupil plane) or in between two beamlines. The increase in image motion could be a problem, but the limiting heat level would be much closer to 15 watts. The source in front of the MEMS plane is effectively double pass because the MEMS is a reflective element. While image motion is not severely impacted for the MEMS plane source, the FWHM of the un-occulted image does seem to increase with increased heat in this position,

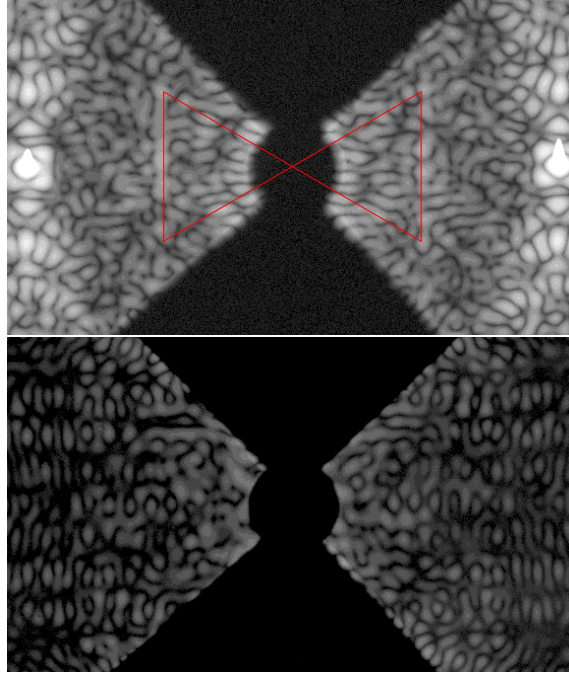


Figure 4. Log-scale far-field images with the MEMS (top) and the flat (bottom) using the new shaped pupil coronagraph, with increased ROI over previous results. The core of the PSF is blocked at focus position 1 to avoid saturating the CCD. In the MEMS image the bright replications of the PSF on the right and left side are caused by the ripple on the MEMS device. The triangles indicate the typical angle for ROI and the spatial frequencies controllable by the MEMS device. The radial averages of both images are shown in Fig. 5.

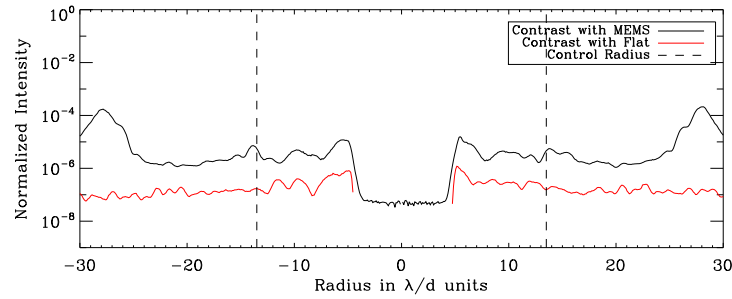


Figure 5. Radial average over 60 degrees of the MEMS and flat mirror high-contrast image. The contrast achieved with the MEMS mirror is slightly worse than predicted by the phase and amplitude measured by the PSDI, possibly caused by increased scatter off of the new mask.

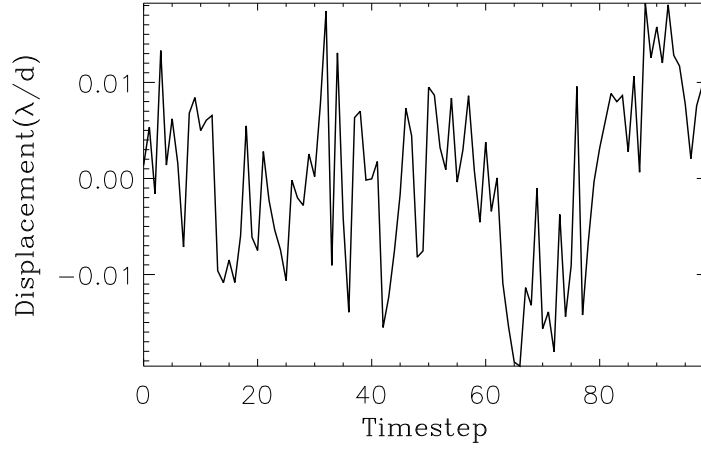


Figure 6. Image motion in the horizontal (x) axis with no heat over 100 frames. The average value of the measurement is subtracted and displacement is converted to λ/D units. There appears to be a somewhat sinusoidal trend over the 100 frames, which is not visible in the shorter 25 frame measurement.

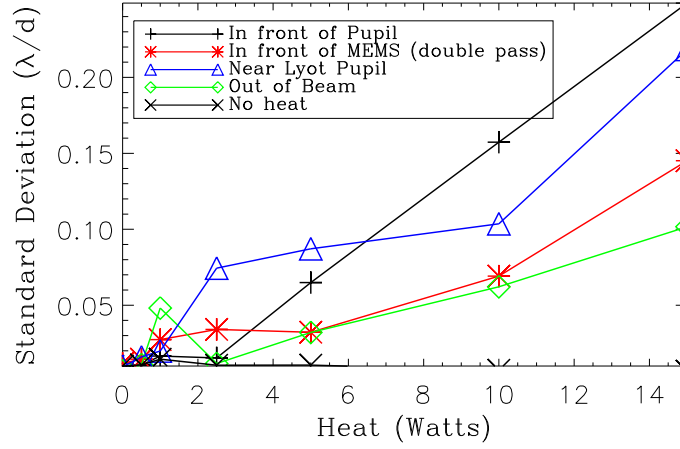


Figure 7. The standard deviation of the horizontal centroid for each 25 frame measurement versus the heat introduced to the system is plotted. The effect of heat on image motion is surprisingly linear, and varies by location. Heat sources near the pupil plane have the largest effect, about $0.02 \lambda/D$ per watt. In the no heat case the data was taken over the same timescales as when the heat source was introduced to ensure there were no systematic effects on those timescales.

which should reduce the effectiveness of the focal plane mask in the occulted data. FWHM is not affected with the source in the other locations tested. The heat source was also placed near focus position 1, but as this data is very similar to the no heat data it was not included in the figure and is likely the best position for an unavoidable heat source to be placed. The no heat data is plotted against watts, and was taken on the same time scales, but the heat source was not engaged.

3.2 Stability in the region of high contrast

Detecting a companion in a high-contrast image is not merely a question of contrast, but also of the stability of the PSF. Experiments on the JPL HCIT have shown the ability to detect companions a factor of 10 below the average PSF halo contrast.³ One way to detect such variations is by doing PSF subtraction; we chose instead to look at the time variations in intensity at a given location in the PSF, expressed as a standard deviation. We also examine the raw contrast in the image, which we would expect to only be affected by very strong heat-induced turbulence. In Fig. 8 the average contrast from 10 to 25 λ/D over 30 degrees on both sides of the PSF core is

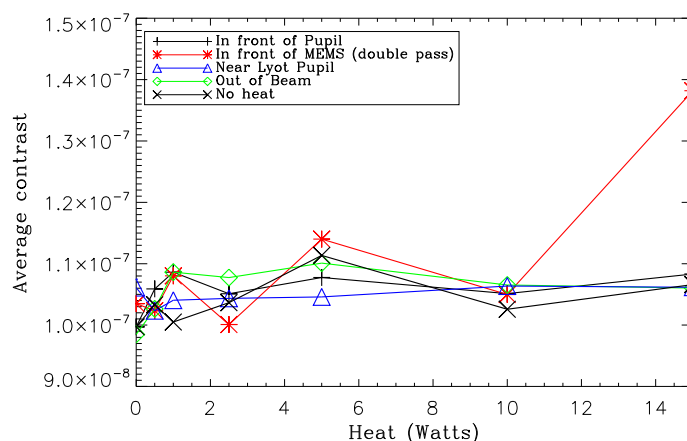


Figure 8. Average contrast from 10 to 25 λ/D over 30 degrees on both sides of the PSF plotted versus heat. In general the amount of heat we introduced is not enough to change the contrast. Introducing 15 watts in front of the MEMS (effectively double pass) does reduce contrast a measurable amount. As before the no heat data was taken on the same time scales as the heat source data, but without introducing heat.

plotted versus heat. In only one location is average contrast affected by the heat source. When the heat source is introduced near the MEMS plane contrast is slightly worse. This could be because of the double pass nature of this location or because of light scattering around the focal plane mask because of the combination of image motion and increased FWHM observed in the un-occulted case.

We can examine the effect of heat on standard deviation in the saturated (occulted) image sequences, just as we calculate the average contrast. One difficulty in analyzing this data is removing image motion. This is not a problem in the images when no extra heat is introduced. Figure 9 is a 25 frame movie of an occulted image without an additional heat source. The images have been normalized based on the unsaturated image, but not registered. There is very little image motion and the speckle pattern appears fairly constant. From examining Fig. 7, we expect the data collected with the heat source near the pupil plane or set at 15 watts near the MEMS plane to be affected by image motion. Figure 10 is a 25 frame measurement with the heat source in front of the MEMS plane set to 15 watts. In the un-occulted image for these conditions we saw an increase in image motion and FWHM which both have the potential to affect contrast. In these images the speckle pattern is clearly changing more than in the no heat case of Fig. 9, but much of the change in the pattern appears to be a shift caused by image motion. This effect is observable in other measurements as well. To separate image motion from other changes in the speckle pattern the occulted images must be registered. The images are registered by calculating the correlation between frames over a small rectangular region on each side of the PSF. Then

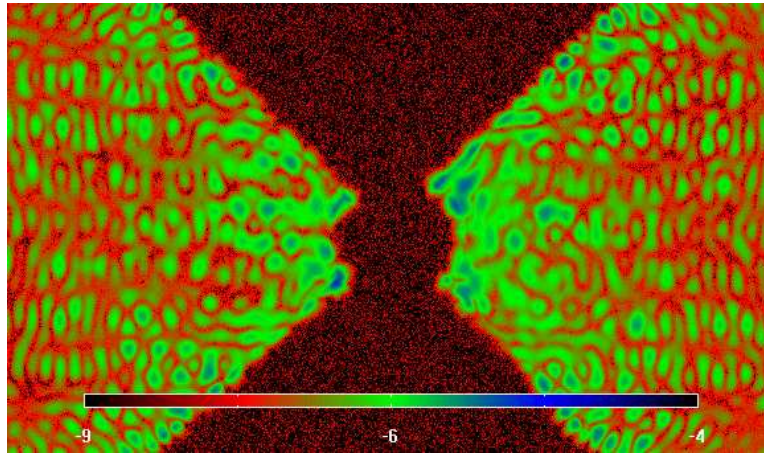


Figure 9. Video 1: A 25 frame movie of an occulted log-scale far-field image without an additional heat source. The images have been normalized to the un-occulted image but not registered. Contrast is approximately 2×10^{-7} . There is very little image motion and the speckle pattern appears constant. <http://dx.doi.org/doi.number.goes.here>

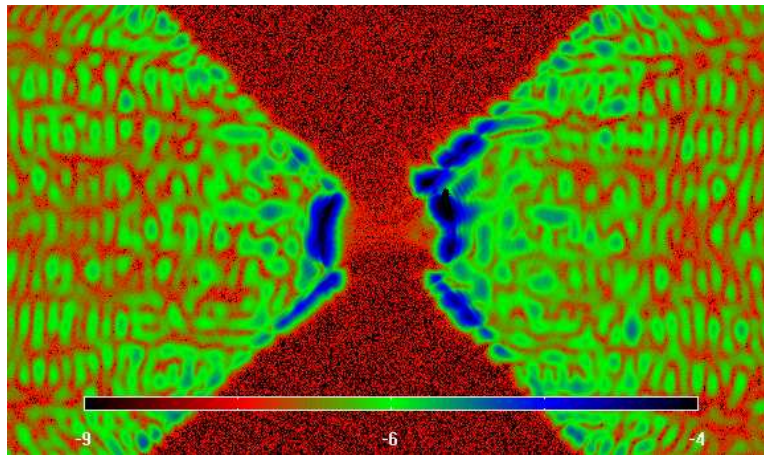


Figure 10. Video 2: A 25 frame movie of the occulted log-scale far-field image with the heat source in front of the MEMS plane set to 15 watts. The speckle pattern appears to be changing, but the changes appear to mostly be shifts caused by image motion. The shifting image and increased FWHM observed in the un-occulted image is apparent as the PSF core is less efficiently blocked by the focal plane mask then in measurements with less heat. <http://dx.doi.org/doi.number.goes.here>

the average of the optimal shift for each side is used to shift the entire image. Image distortion and changes in the speckle pattern that we might see as a result of the additional heat source could limit the robustness of this technique. This is particularly true close to the core of the image where image motion can produce more significant changes with increased light scatter around the focal plane mask. The region used to register the image is from 10 to 25 λ/D in order to avoid the region close to the core. Figure 11 is a movie of registered frames from a measurement with the heat source close to the pupil. Most image motion appears to be removed,

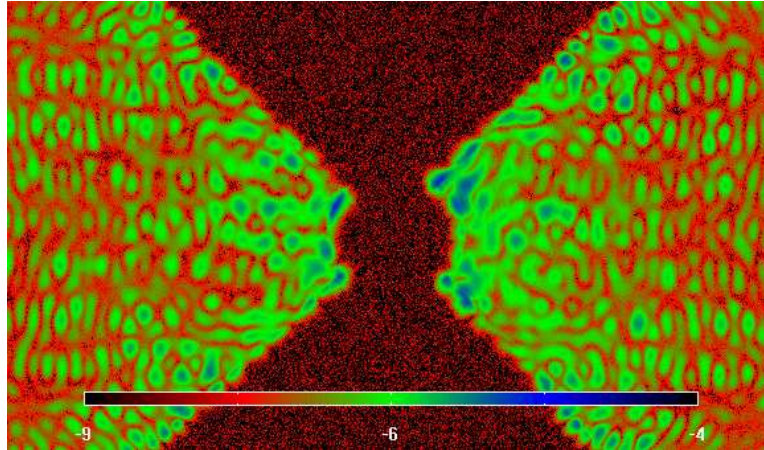


Figure 11. Video 3: A 25 frame movie of the occulted log-scale images measured with the heat source in front of the pupil plane set to 15 watts. These images have been registered based on the correlation of the speckle pattern. Most image motion appears to be removed, but it is not clear that there is no residual image motion that would affect measurements of standard deviation in the speckle pattern. <http://dx.doi.org/doi.number.goes.here>

but it is not clear that there is no residual image motion that would affect measurements of standard deviation in the speckle pattern. It does appear that some speckles get brighter or darker over time indicating that some changes outside of image motion are taking place in the speckle pattern. One way to quantify this variation is to take the standard deviation of each pixel over time in the registered images. To reduce noise we have averaged the standard deviation in time over the same ROI used to calculate the average contrast (10-25 λ/D over 30 degrees on both sides of the PSF). The average standard deviation over this region is plotted versus the heat for each location of the heat source (See Fig. 12). It is possible that the increase in standard deviation is only a result of the corresponding increase in image motion with heat. It is interesting however that the lyot pupil plane and the MEMS plane have the largest increase in standard deviation of contrast, while the pupil plane was the worst for image motion. Figure 13 is a plot of the image motion versus the standard deviation of the high-contrast region for each measurement. There does not appear to be any notable correspondence between image motion and standard deviation across the measurements. The region used for registering the images is narrow rectangle on both sides of the image. The best shift for each of these rectangles is calculated and then the average of the two is applied to the frame. To see if an improvement in image registration would reduce the increase in standard deviation with heat we repeated the registration only using the rectangle on one side of the image, and then only averaged the standard deviation in time over that smaller region. The results are largely the same as presented in Fig. 12. The combination of these calculations and the apparent reduction in image motion of the registered frames, while not conclusive, largely convinces us that there is an increase in standard deviation of the speckle pattern with small heat sources.

3.3 Apodized Pupil Lyot Coronagraph Stability

The GPI instrument will use an APLC for diffraction suppression instead of the shaped pupil coronagraph that is often used in testbed experiments and testing of the APLC on the testbed is ongoing.¹⁵ In the shaped pupil stability measurements image motion reduces the efficiency of the focal plane mask because when the core is not centered more light scatters into the ROI. For the APLC, the occulter is well-matched to the apodizer and the lyot stop making image motion potentially more damaging. The stability measurement with the heat source at

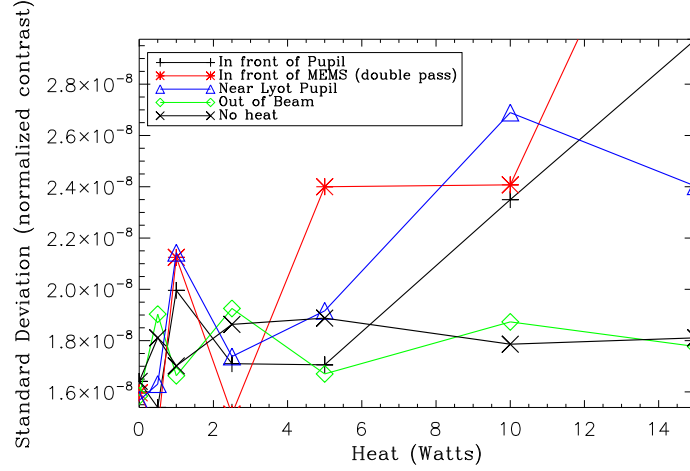


Figure 12. The standard deviation over the 25 frames taken at each heat level, averaged over the a 30 degree region from 10 to 25 λ/D on both sides of the PSF is plotted versus heat for each location of the source. The images were registered prior to the calculation of standard deviation which should greatly reduce the effect of image motion, but residual image motion could still affect the calculation.

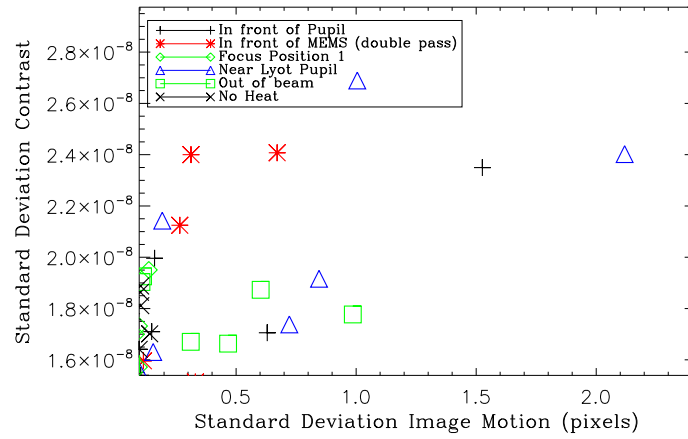


Figure 13. The standard deviation from Fig. 12 is plotted versus the image motion from Fig. 7. If residual image motion is the main source of the increase in standard deviation you would expect the correlation between motion and standard deviation to be the same for all heat source locations. This data suggests that image motion is not the sole cause of the increase in standard deviation with heat.

the pupil plane was repeated with the APLC instead of the shaped pupil. As expected image motion remains the same as the shaped pupil case, but the occulted images look quite different. Figure 14 is the image with no additional heat. The speckle pattern looks as expected and is as stable as the shaped pupil measurements. (For more information on measurements with the APLC see Thomas et al in this volume¹⁵). The image when the heat source in the pupil plane set to 15 watts looks quite different. In the shaped pupil case the image has additional scatter around the core and the speckle pattern remains approximately the same, but in the APLC image the speckle pattern is no longer visible because of diffraction around the core. Average contrast is reduced by more than an order of magnitude.

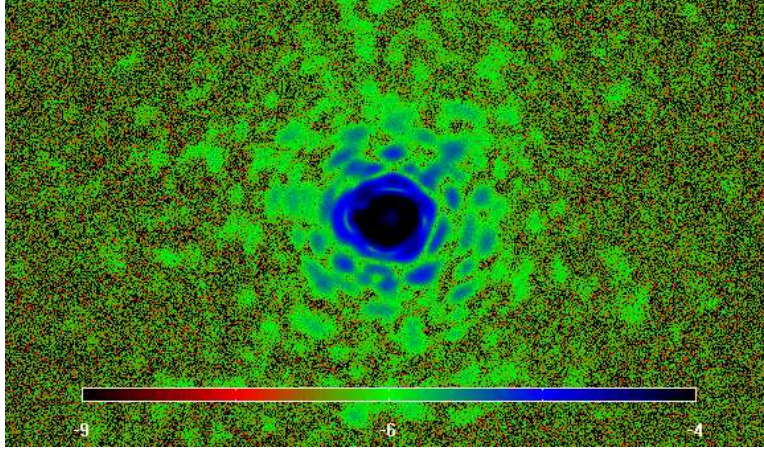


Figure 14. Log-scale high-contrast image using the APLC to suppress diffraction (with flat mirror). The speckle pattern looks roughly as expected and the stability is comparable to the shaped pupil tests.

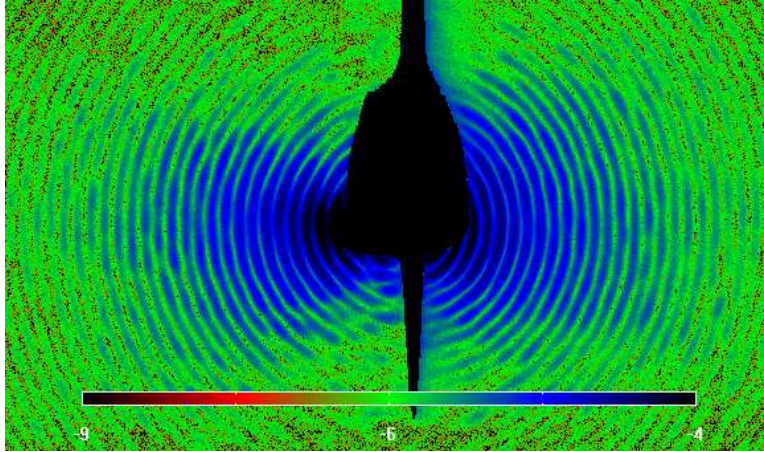


Figure 15. Log-scale high-contrast image with the APLC with a 15 watt heat source in front of the pupil plane. In this image diffraction dominates the image and speckle pattern of Fig. 14 is not visible.

4. CONCLUSIONS AND FUTURE WORK

From these stability measurements on the ExAO testbed we conclude that heat sources in the pupil or re-imaged pupil planes are likely to cause the most damage to high-contrast imaging with image motion increasing by $0.02 \lambda/D$ per watt of energy. Sources higher than 5 watts should be avoided. The safest place to introduce heat sources of greater than five watts is near a focal plane. With more heat, approximately 15 watts, changes in FWHM can also be observed. In general these results must be scaled to understand the effect of heat on systems with a different beam size.

There also appears to be a relationship between increased heat at specific locations and standard deviation in the ROI of a high-contrast image, but in the final instrument design speckle variation introduced by other sources should be more significant. However image motion cannot be as easily decoupled from APLC images and should be kept to a minimum to avoid reducing contrast.

The ExAO testbed will continue to investigate high-contrast imaging in support of GPI. In particular future experiments will focus on the APLC and an upgrade to a 4096-actuator MEMS device for wavefront control. Figure 16 is a picture of the first engineering grade 4096 actuator MEMS delivered by Boston Micromachines to the LAO in April 2008.

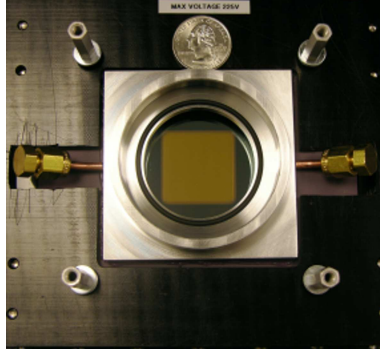


Figure 16. Picture of first engineering grade 4096-actuator MEMS device delivered by Boston Micromachines to the LAO in April 2008.

ACKNOWLEDGMENTS

Contact Julia Evans at evans74@llnl.gov. We are grateful to R. Belikov and Princeton University's Terrestrial Planet Finder group for providing us with the shaped pupil mask. This work has been supported in part by the Gordon and Betty Moore Foundation through its grant to the UCO/Lick Laboratory for Adaptive Optics and in part by the National Science Foundation Science and Technology Center for Adaptive Optics, managed by the University of California at Santa Cruz under cooperative agreement No. AST-9876783. This work performed under the auspices of the U.S. Department of Energy by Lawrence Livermore National Laboratory under Contract DE-AC52-07NA27344. LLNL-PROC-404640

REFERENCES

1. B. Macintosh, *et al.*, *Comptes rendus-Physique* **8**(3-4), pp. 365–373, 2007.
2. F. Wildi, *et al.*, in *Astronomical Adaptive Optics Systems and Applications III*, R. K. Tyson and M. Lloyd-Hart, eds., *Proc. SPIE* **6691**, p. 66910L, 2007.
3. J. Trauger and W. Traub, *Nature* **446**(7137), pp. 771–3, 2007.
4. S. Thomas, *et al.*, in *MEMS Adaptive Optics II*, S.S. Olivier, T.G. Bifano and J.A. Kubby, eds., *Proc. SPIE* **6888**, p.68880J, 2008.
5. J. W. Evans, G. Sommargren, B. A. Macintosh, S. Severson, and D. Dillon, *Optics Letters* **31** No.5, pp. 565–567, 2006.
6. J. Evans, *et al.*, D. R. Coulter, ed., *Proc. SPIE* **6693**, p. 669312, 2007.
7. T. Bifano, P. Bierden, and J. Perreault, in *Advanced Wavefront Control: Methods, Devices and Applications II*, J. D. Gonglewski, M. T. Grueneisen, and M. K. Giles, eds., *Proc. SPIE* **5553**, pp. 1–16, 2004.
8. J. W. Evans, *et al.*, *Optics Express* **14**, pp. 5558–5570, 2006.
9. L. Poyneer, D. Dillon, S. Thomas, and B. Macintosh, *Applied Optics* **47**(9), pp. 1317–1326, 2008.
10. N. J. Kasdin, R. J. Vanderbei, D. N. Spergel, and M. G. Littman, *Astrophysical Journal* **582**(2), pp. 1147–61, 2003.
11. R. Belikov, *et al.*, *Proceedings of the International Astronomical Union* **1**(C200), pp. 415–420, 2006.
12. K. Balasubramanian, *et al.*, in *Space Telescopes and Instrumentation I: Optical, Infrared, and Millimeter*, J. C. Mather, H. A. MacEwen, and M. W. M. de Graauw, eds., *Proc. SPIE* **6265**, p. 62653N, 2006.
13. R. Soummer, C. Aime, and P. E. Falloon, *EAS Publications Series, Volume 8, 2003, Astronomy with High Contrast Imaging, Proceedings of the conference held 13-16 May, 2002 in Nice, France. Edited by C. Aime and R. Soummer*, pp.93-105. **8**, pp. 93–105, 2003.
14. C. Aime, R. Soummer, and A. Ferrari, *A&A* **379**, pp. 697–707, Nov. 2001.
15. S. J. Thomas, *et al.*, in *Adaptive Optics Systems*, N. Hubin, C. Max and P. Wizinowich, eds., *Proc. SPIE* **7015**, in press. 2008.